JACS
JOURNAL OF THE AMERICAN CHEMICAL SOCIETY
pubs.acs.org/JACS
Article

Interpenetrating 3D Covalent Organic Framework for Selective Stilbene Photoisomerization and Photocyclization

Tao-Yuan Yu, Qian Niu, Yifa Chen,* Meng Lu, Mi Zhang, Jing-Wen Shi, Jiang Liu, Yong Yan,* Shun-Li Li, and Ya-Qian Lan*

Cite This: J. Am. Chem. Soc. 2023, 145, 8860–8870
Read Online

ABSTRACT: The selective photoisomerization or photocyclization of stilbene to achieve value upgrade is of great significance in industry applications, yet it remains a challenge to accomplish both of them through a one-pot photocatalysis strategy under mild conditions. Here, a sevenfold interpenetrating 3D covalent organic framework (**TPDT-COF**) has been synthesized through covalent coupling between *N*,*N*,*N*,*N*-tetrakis(4-aminophenyl)-1,4-benzenediamine (light absorption and free radical generation) and 5,5′-(2,1,3-benzothiadiazole-4,7-diyl)bis[2-thiophenecarboxaldehyde] (catalytic center). The thus-obtained sevenfold interpenetrating structure presents a functional pore channel with a tunable photocatalytic ability and specific pore confinement effect that can be applied for selective stilbene photoisomerization and photocyclization. Noteworthily, it enables photogeneration of *cis*-stilbene or phenanthrene with >99% selectivity by simply changing the gas atmosphere under mild conditions (Ar, $Sele_{Cis}$. > 99%, $Sele_{Phen}$. < 1% and O_2, $Sele_{Cis}$. < 1%, and $Sele_{Phen}$. > 99%). Theoretical calculations prove that different gas atmospheres possess varying influences on the energy barriers of reaction intermediates, and the pore confinement effect plays a synergistically catalytic role, thus inducing different product generation. This study might facilitate the exploration of porous crystalline materials in selective photoisomerization and photocyclization.

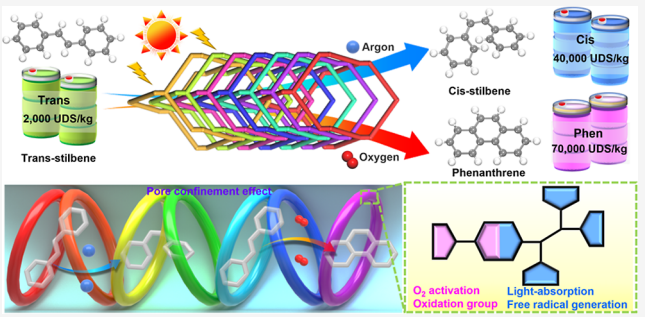

INTRODUCTION

Stilbene and its derivatives, possessing unique chemical scaffolds in biologically active entities, are versatile starting materials for numerous chemical transformations, yet the stereoselective construction of value-added products remains a conspicuous and challenging task in industrial fields.[1−4] During the past years, much effort has been made to develop strategies that enable the stereoselective transformation of stilbene for potential applications in scintillators, chromatic lasers, industrial dyes, anticancer drugs, and so forth.[5−7] Especially in the biomedicine field, precise control of the stereochemistry regarding *E*/*Z* isomers personates a crucial status.[8,9] Notably, *trans*-stilbene as a kind of typical stilbene-derived compound can be used as an important precursor for the photoisomerization generation of *cis*-stilbene or further undergoing established conrotatory 6π electrocyclization to produce phenanthrene.[10,11] During this process, *cis*-stilbene with ∼40,000 USD/kg (based on the real-time market price of September 2022 in China) market value is commonly presented in natural plants with very low contents, and its extraction or separation from natural products is expensive in cost, which is much necessary to selectively synthesize *cis*-stilbene through more efficient and practical methods. In general, there are some commonly applied methods for the production of *cis*-stilbene in the industry including Wittig reactions, Peterson olefination, cross-coupling of alkenyl halides, Shapiro reactions, *Z*-isomer metathesis, and so forth.[12−16] However, these reaction methods still suffer from problems like poor product selectivity, complex post-treatment, environmental pollution, and so forth.[17,18] Meanwhile, another value-added product, phenanthrene, has a higher market value (∼70,000 UDS/kg). However, its production from coal tar usually contains multistep distillation processes that require large amounts of solvent, the use of interferents, and inevitable safety concerns (e.g., internal pressure arising from the product attachment), resulting in high cost and difficulty in purification.[19,20] In addition to the commonly applied complex distillation process, other methods (e.g., Scholl/Mallory reactions, Bardhan-Sengupta, etc.)[21−24] have also been explored for phenanthrene production, yet they still have bottlenecks like the utilization of excess acids (e.g., TfOH,

Received: November 20, 2022
Published: April 18, 2023

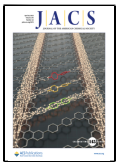

Scheme 1. Schematic Diagram of the Interpenetrating COF Structure for Selective *trans*-Stilbene Photoisomerization and Photocyclization; (a) Schematic Diagram of the Possible Factors in COFs for *trans*-Stilbene Value Upgrade; (b) Pore Confinement Effect and Possible Functions of Struts for *trans*-Stilbene Value Upgrade

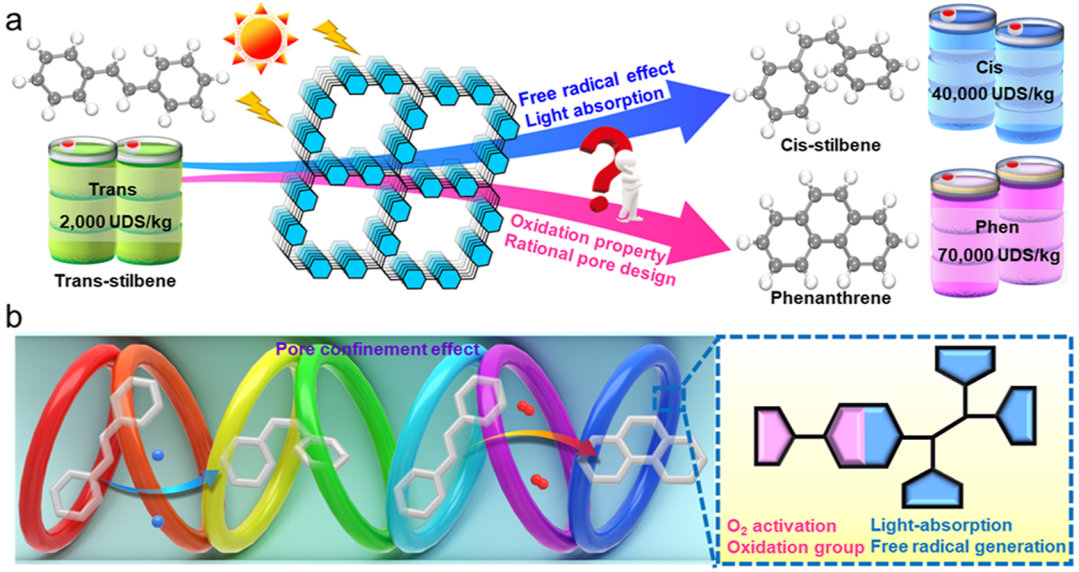

$AlCl_3$, $FeCl_3$, $MoCl_5$, etc.) or strong oxidants [e.g., KI, I_2, 2,3-dichloro-5,6-dicyano-1,4-benzoquinone (DDQ), etc.], bringing about a host of waste byproducts and low efficiency.[25−28] At present, despite the intensive investigation, the exploration of suitable catalysis systems to accomplish the selective isomerization or cyclization of *trans*-stilbene through one-pot reaction methods, especially those that can be conducted under green and economic conditions, remains a daunting challenge.

The photocatalysis reaction, a kind of novel and environmentally benign technique that can combine light energy with typical organic synthesis, has arisen to be a promising strategy for selective isomerization or cyclization of *trans*-stilbene.[29−31] At present, various photocatalysts have been explored to promote photocatalytic *trans*-stilbene isomerization, such as metal photocatalysts (e.g., Ir- or Pd-based catalysts),[30,32] (−)-riboflavin,[33] alkaline catalysts (e.g., NaOH, $NaHCO_3$, etc.),[3,4] ketones (e.g., *para*-benzoquinone, 2-iodo-9-fluorenone, etc.),[35,36] or condensed nucleus compounds (e.g., SiO_2@(−)-riboflavin).[37] Nevertheless, there are some unsolved issues: (i) most strategies rely on isomeric kinetic control of the reactions[38] with commonly applied high-energy reagents (e.g., $TMSCH_2Li$, etc.),[39−41] (ii) *trans*-stilbene photoisomerization reactions are generally based on noble metal catalysts and often require harsh conditions (e.g., strongly alkaline, low temperature, etc.),[34,35] and (iii) it is usually accompanied by the generation of byproducts (e.g., 1,2,3,4-tetraphenylcyclobutane) that are difficult to be removed under light illumination.[42,43] In addition, the photoderivatization reaction based on *E*-to-*Z* photoisomerization of *trans*-stilbene, such as the formation of phenanthrene, has been rarely studied. Henceforth, the exploration of cost-effective, stable, visible-light responsive, and efficient photocatalysts is highly pursued for selective *trans*-stilbene photoisomerization and photocyclization to achieve value upgrades.

Covalent organic frameworks (COFs) are a rising class of porous crystalline materials based on covalent linking interactions, showing the properties of designable structures, large surface area, well-defined crystalline structures, tunable functionality, low density, and so forth.[44−47] Due to the tunability of the COF structures, it is noted that the required functions can be easily designed, thus enabling them to be promising platforms for potential applications in gas sorption and separation, energy transformation, and heterogeneous catalysis.[48,64] Specifically, these characteristics can render interesting structural characteristic research platforms as photocatalysts for photoisomerization or photocyclization of *trans*-stilbene owing to the following reasons: (i) compared with other materials with higher density, COFs with a similar quality might provide more exposed surface area and active sites; (ii) the pore structures (e.g., pore size, inner pore environments, or interpenetration degree) can be specially designed with possible pore confinement effects;[48] and (iii) specifically selected functional groups can confer the COF structures with light adsorption, suitable band gap, and photo-oxidation ability that are conducive to generating free radicals for selective *trans*-stilbene photoisomerization or photocyclization.[49] Prior to this, although some examples like TpTt COF have been reported that can be applied for *E*-to-*Z* photoisomerization of *trans*-stilbene,[50] the exploration of selective *trans*-stilbene photoisomerization and even photocyclization remains at an early stage. Therefore, it would be much necessary to develop powerful COF-based photocatalysts that can accurately regulate the porosity, functionality, or light-absorption ability to meet the stringent requirements for highly selective *trans*-stilbene photoisomerization and photocyclization.

Herein, we have prepared a kind of sevenfold interpenetrating 3D-COF (denoted as **TPDT-COF**) based on the covalent connection of *N*,*N*,*N*,*N*-tetrakis(4-aminophenyl)-1,4-benzenediamine (TAPB) and 5,5′-(2,1,3-benzothiadiazole-4,7-diyl) bis[2-thiophenecarboxaldehyde] (DTBT) and successfully applied it in highly selective *trans*-stilbene photoisomerization and photocyclization (Scheme 1). TAPB is a small molecule with a Wurster-type structure, which can be readily transferred into a triple-excited state with double radical properties under photo- or thermal conditions.[51−53] DTBT is a strong redox molecule, which can act as an excellent O_2 activation and photo-oxidation group.[54] Its combination with

https://doi.org/10.1021/jacs.2c12313
J. Am. Chem. Soc. 2023, 145, 8860−8870

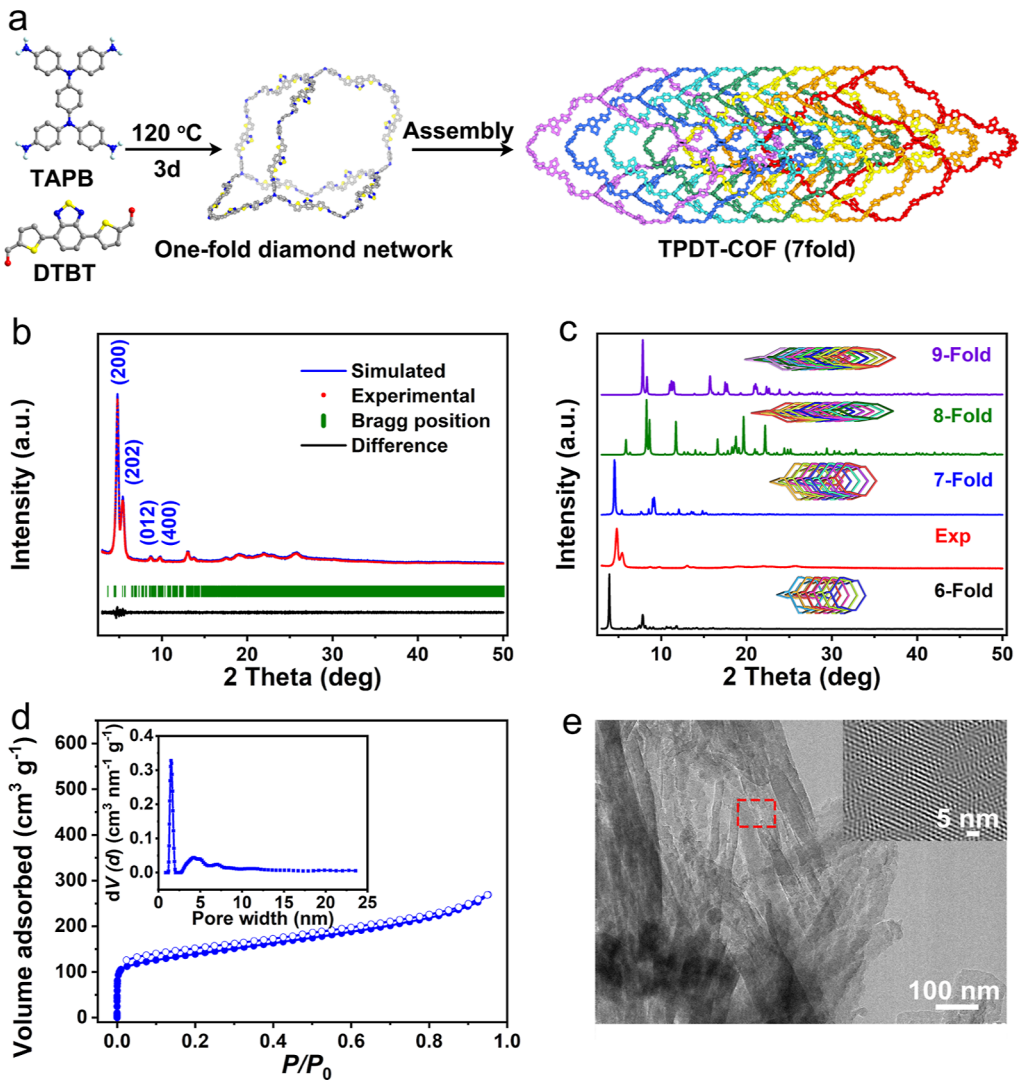

Figure 1. Characterizations of **TPDT-COF**. (a) Synthesis and structure of **TPDT-COF**. (b) Experimental, Pawley-refined, and simulated PXRD patterns of **TPDT-COF**. (c) Experimental and simulated PXRD patterns of **TPDT-COF** with different interpenetrating structures (i.e., sixfold, sevenfold, eightfold, and ninefold). (d) N_2 sorption curve of **TPDT-COF** at 77 K (inset is the pore size distribution profile). (e) TEM and lattice fringe images of **TPDT-COF** (inset is the Fourier transform image of the circled place).

a specially designed sevenfold interpenetrating structure can endow it with a pore confinement effect, visible-light-adsorption ability, and suitable functions that enable selective *trans*-stilbene photoisomerization and photocyclization. Noteworthily, it can achieve the photogeneration of *cis*-stilbene or phenanthrene with >99% selectivity by simply changing the gas atmosphere under mild photocatalysis conditions (Ar, $Sele_{Cis.}$ > 99%, $Sele_{Phen.}$ < 1% and O_2, $Sele_{Cis.}$ < 1%, and $Sele_{Phen.}$ > 99%), during which the market value of *trans*-stilbene (~2,000 USD/kg) can be ~20 and ~35 times upgraded for *cis*-stilbene (~40,000 USD/kg) and phenanthrene (~70,000 USD/kg), respectively. Based on the experimental results and density functional theory (DFT) calculations, we illustrate the vital roles of the pore confinement effect and functional struts in **TPDT-COF** that contribute to the unique and superior photocatalytic performance. This work would pave a new way in exploring porous crystalline catalysts for highly selective *trans*-stilbene photoisomerization and photocyclization.

RESULTS AND DISCUSSION

Synthesis and Structure of TPDT-COF. The synthesis of **TPDT-COF** was carried out through the Schiff-base condensation reaction of TAPB and DTBT, and a kind of black powder was obtained after 72 h at 120 °C (Figure 1a, for details, see the Supporting Information). To define the crystalline structure of **TPDT-COF**, powder X-ray diffraction (PXRD) of the as-synthesized **TPDT-COF** was first assessed by theoretical structural simulations. In general, the 1,4-bis(diphenylamino)benzene (DAB) unit can adopt two configurations: one is square with C_{2h} symmetry, and the other is tetrahedral with D_{2d} symmetry (Figure S1). Both configurations of DAB have been seen in single-crystal X-ray structures of metal−organic frameworks assembled from the tetracarboxylate linkers containing the DAB unit.[55,56] The structure of **TPDT-COF** was modeled as a sevenfold diamond (**dia**) topology based on the geometrical connectivity of the two individual units. The experimental PXRD pattern showed good agreement with the calculated one based on the structural model (Figure 1b). Pawley refinements revealed

https://doi.org/10.1021/jacs.2c12313
J. Am. Chem. Soc. 2023, 145, 8860−8870

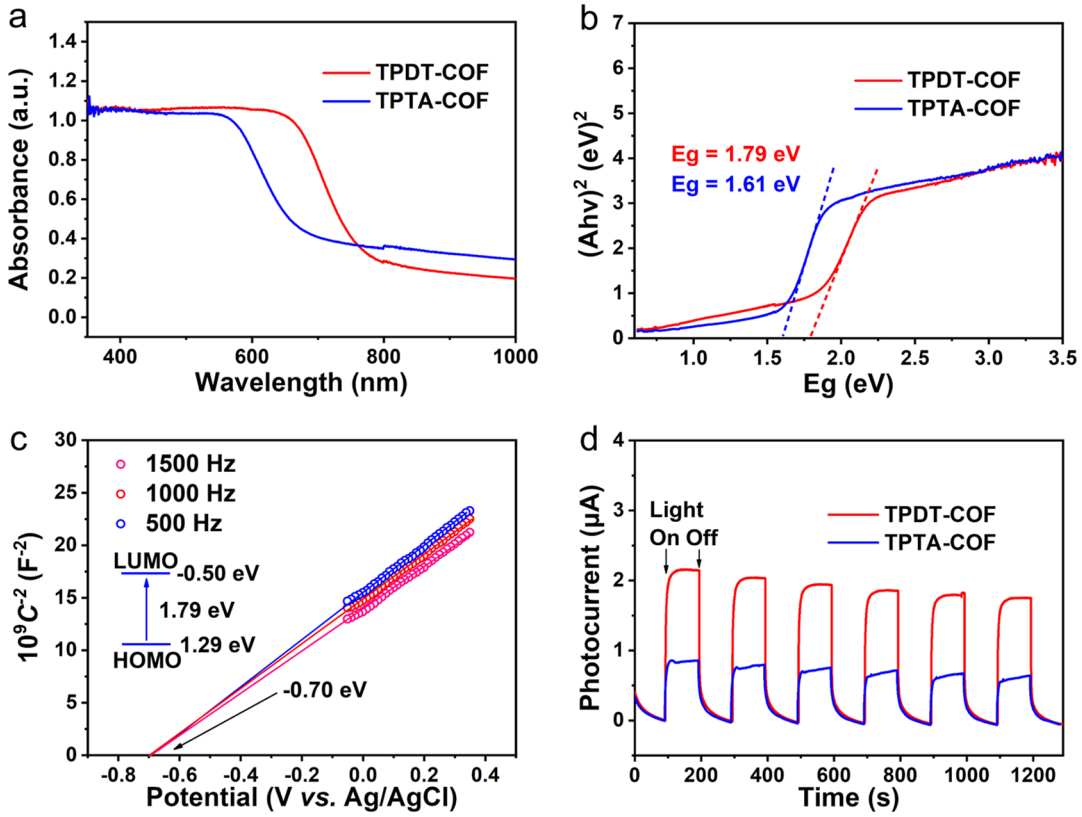

Figure 2. Optical property of **TPDT-COF** and **TPTA-COF**. (a) Solid-state UV/vis spectra of **TPDT-COF** and **TPTA-COF**. (b) Tauc plot for band gap calculation of **TPDT-COF** and **TPTA-COF**. (c) Mott−Schottky plots of **TPDT-COF** with an inset energy diagram of the LUMO and HOMO levels. (d) Transient photocurrent response of **TPDT-COF** and **TPTA-COF**.

the unit-cell parameters (*P*2 space group, a = 38.351 Å, b = 11.995 Å, and c = 43.678 Å, $\alpha = \gamma = 90°$, and β = 71.544°), which matched well with the modeled structure (R_p = 3.7% and R_{wp} = 4.6%). Meanwhile, except for **dia** topology, we have also considered other possible structures like **kgm** or **sql** topology (Figures S2 and S3). However, the PXRD patterns for these structures did not match the experimental ones (Figures S2 and S3). To further prove the sevenfold model and get rid of other possible interpenetrating ones, the interpenetrating models from sixfold to ninefold of **TPDT-COF** have also been analyzed by theoretical structural simulation and we found that it was indeed a kind of sevenfold interpenetrating structure based on the matching degree of experimental PXRD patterns and simulated ones (Figure 1c).

In the PXRD pattern of **TPDT-COF**, it has intense peaks at 4.58, 5.44, 8.47, and 9.24°, which can be assigned to the (2, 0, 0), (2, 0, 2), (0, 1, 2), and (4, 0, 0) facets of **TPDT-COF**, respectively (Table S1). Based on the above results, **TPDT-COF** was proposed to have the expected architectures with a sevenfold interpenetrating diamond (**dia**) topology. In the onefold structure, its porous cavity has a diameter of ∼21 Å (Figure 1a). Interestingly, the interpenetrating effect largely restricts the pore channel and a kind of irregular inner surface can be viewed from the b axis with an aperture of ∼13 Å in the sevenfold structure. Specifically, the functional groups of DTBT protruded diagonally and pointed to the pore center, thus creating a complex and diversified pore environment. From the a or c axis, it was interpenetrated with limited or inaccessible porosity, thus creating a kind of perfect pore environment that might possess a pore confinement effect for the possible application in highly selective photocatalysis (Figure S4).

The structure of **TPDT-COF** was further investigated by various characterizations. Solid-state ^{13}C cross-polarization magic-angle spinning nuclear magnetic resonance (^{13}C CP/MAS NMR) spectra revealed that the peak at 151 ppm was ascribed to the carbon atom of the imine bond, implying the successful formation of the covalent bond (Figure S5).[57] In Fourier transform infrared (FT-IR) spectra, the C═N stretching vibration band was detected at 1625 cm^{-1} in **TPDT-COF** (Figure S6).[58] Meanwhile, the C═O stretching vibration band (1700 cm^{-1}) and $-NH_2$ vibration band (3200−3500 cm^{-1}) belonging to the comparative reactant monomers decreased obviously for **TPDT-COF** in the spectra, implying the successful generation of covalent bonds. In comparison, **TPTA-COF** was also synthesized and characterized as supported by the PXRD and FT-IR tests (Figures S7 and S8).[59] For **TPTA-COF**, it was assembled by the same TAPB linker, while DTBT was replaced by terephthalaldehyde (TA), which could serve as a desired contrast sample to reflect the importance of DTBT in **TPTA-COF** (Figure S7a). Besides, the porosity of **TPDT-COF** was also tested by N_2 sorption measurements at 77 K (Figure 1d). The Brunauer−Emmett−Teller surface area (S_{BET}) and total pore volume of **TPDT-COF** were calculated to be 498 $m^2\ g^{-1}$ and 0.417 $cm^3\ g^{-1}$, proving the porous nature of the structure.[60] Moreover, the pore size distribution of **TPDT-COF** showed that it mainly centered at ∼1.5 nm, which was basically in conformity with the calculated results as mentioned above (Figure 1d, insert image).[61] Thus, we have obtained a kind of interpenetrating structure that possesses accessible and limited pore channels,

https://doi.org/10.1021/jacs.2c12313
J. Am. Chem. Soc. 2023, 145, 8860−8870

which might serve as an excellent platform with a pore confinement effect to study relative structure−function relationships.

Generally, stability is a vital factor to evaluate the basic property of **TPDT-COF** as it determines the durability of photocatalysts. The thermal stability of **TPDT-COF** and **TPTA-COF** was evaluated by thermogravimetric analyses, and no obvious weight changes were detected up to ∼350 °C (Figure S9). To test the chemical stability, **TPDT-COF** was selected as the example and tested by immersing it in different solvents [e.g., *N*,*N*-dimethylformamide (DMF), tetrahydrofuran, acetone, acetonitrile, methanol, and H_2O] for more than 7 days and the obtained samples were characterized by the PXRD and FT-IR tests[62] (Figures S10 and S11). The results indicated that it could retain its structural integrity after treatment with these solvents when compared with the initial states, suggesting the high chemical stability of the covalent-bonding structure. Furthermore, scanning electron microscopy and transmission electron microscopy (TEM) were further utilized to characterize the morphology of **TPDT-COF** and **TPTA-COF**. Interestingly, **TPDT-COF** displayed a nanorod morphology (length, ∼500 nm) (Figures 1e and S12), which was different from that of **TPTA-COF** (nanosheet stacking morphology, ∼1.5 μm) (Figure S13). We further studied the crystallinity of the COFs by high-resolution TEM (HR-TEM) tests.[63] Taking **TPDT-COF**, for instance, the oriented lattice fringes of **TPDT-COF** could be clearly observed in the HR-TEM image, indicating the high crystallinity of TPDT-COF (Figure 1e, insert image).

Characterizations of the Optical Properties of TPDT-COF. UV/vis diffuse reflectance spectroscopy (DRS) and ultraviolet photoelectron spectroscopy (UPS) tests were conducted to determine the basic optical property of **TPDT-COF** and **TPTA-COF**. DRS spectra showed that **TPDT-COF** had an absorption range from ∼400 to ∼800 nm, which was much wider than that of **TPTA-COF** (∼400 to ∼650 nm). This result indicated that the DTBT unit in **TPDT-COF** was more favorable in enhancing the light-adsorption ability than that of the TA unit in **TPTA-COF** (Figures 2a and S14). Besides, their relative band gaps were studied based on the UPS results. The corresponding band gaps (E_g) were calculated to be 1.79 eV for **TPDT-COF** and 1.61 eV for **TPTA-COF** by the Tauc plots, respectively (Figure 2b), suggesting their characteristics of semiconductor-like materials.[64] In addition, Mott−Schottky measurements were further performed to determine the band positions of **TPDT-COF** and **TPTA-COF**; the results were consistent with those from the UPS tests (Figures 2c and S15−S17).

Additionally, transient photocurrent tests were also carried out. Interestingly, the intensity of the transient photocurrent response of **TPDT-COF** was much higher than that of **TPTA-COF**, implying that the assembly of TAPB and DTBT in **TPDT-COF** could result in higher photoinduced electron separation and transport efficiency (Figure 2d). In addition, electrochemical impedance spectroscopy was performed to investigate the charge transfer resistance (Figure S18). The Nyquist plots demonstrated that **TPDT-COF** had much smaller charge transfer resistance than **TPTA-COF** as supported by its smaller semicircle in the high-frequency region. The results indicated that the covalent connection between TAPB and DTBT in **TPDT-COF** might effectively facilitate the electron−hole separation and prevent its recombination. Thus, we have obtained a kind of sevenfold interpenetrating 3D **TPDT-COF** that possessed excellent photochemical properties, which might hold much promise for selective *trans*-stilbene photoisomerization and photocyclization.

Photocatalytic Performances of Samples. To evaluate the photocatalytic property, the reactions were conducted at room temperature and normal pressure under xenon lamp irradiation with the full spectrum (Figure 3a,b, for details, see the Supporting Information). First, an O_2 atmosphere was applied to study the basic photocatalytic property with different reaction times. At 4 h, a 51% $Conv_{Trans}$. with a $Sele_{Cis}$. of 96% was detected, and the remaining product was phenanthrene (selectivity, 4%) (Figure 3c). From 4 to 12 h, the $Conv_{Trans}$. and $Sele_{Phen}$. gradually increased along with the reaction time. Interestingly, the maximum conversion efficiency (100%) with $Sele_{Phen}$. 99% could be achieved at 16 h and the results remained almost intact with a longer reaction time (e.g., 18 or 24 h) (Table S2). Therefore, we selected 16 h as the desired reaction time to further evaluate other properties. Moreover, the performances using various solvent types [i.e. DMF, *N*,*N*-dimethylacetamide (DMA), toluene, 1,4-dioxane (DOA), and acetonitrile (MeCN)] have also been characterized (Table S3). The results show that DMF was the optimal solvent for this transformation, and the achieved performance ($Conv_{Trans}$. 100%, $Sele_{Phen}$. 99%, and $Sele_{Cis}$. 1%) was superior to that of other solvents like DMA ($Conv_{Trans}$. 90%, $Sele_{Phen}$. 27%, and $Sele_{Cis}$. 63%), toluene ($Conv_{Trans}$. 81%, $Sele_{Cis}$. 75%, and $Sele_{Phen}$. 25%), DOA ($Conv_{Trans}$. 88%, $Sele_{Cis}$. 45%, and $Sele_{Phen}$. 55%) or MeCN ($Conv_{Trans}$. 72%, $Sele_{Cis}$. 84%, and $Sele_{Phen}$. 16%). In addition, we further explored the influence of the DMF amount (i.e., 0−3 mL) on the performance and the result showed that 1 mL was the optimal one for this transformation. Based on the optimization of the basic conditions, we have also tested the performances of various contrast samples (Figure 3d and Table S2). Specifically, the $Sele_{Phen}$. of **TPTA-COF** was detected to be 10%, which was lower than that of **TPDT-COF**. This result was compiled with the better photoproperty as mentioned above and proved the superiority of the sevenfold 3D structure that was constructed from TAPB and DTBT linkers in efficient photocatalysis. Moreover, the performances of the relative monomers (i.e., TAPB, DTBT, and their mixture) were also characterized. In detail, TAPB ($Conv_{Trans}$. 86%, $Sele_{Phen}$. 20%, and $Sele_{Cis}$. 80%), DTBT ($Conv_{Trans}$. 95%, $Sele_{Cis}$. 58%, and $Sele_{Byproduct}$. 42%), and the mixture of TAPB and DTBT ($Conv_{Trans}$. 73%, $Sele_{Phen}$. 36%, and $Sele_{Cis}$. 64%) all showed much lower performances than that of **TPDT-COF**, indicating the advantages of sevenfold interpenetrating 3D structure.

Moreover, we have proved the effect of pore confinement by preparing an amorphous material using similar raw materials by reducing the maturation period and changing the solvent from benzyl alcohol to DMF. The PXRD pattern with broad peak and FI-IR spectra prove the successful synthesis of a kind of amorphous material (Figure S19). Based on the amorphous material, we have explored its performance in selective photoisomerization and photocyclization. The results show that it displays poorer properties under an Ar atmosphere ($Conv_{Trans}$. 67%, $Sele_{Cis}$. 99%, and $Sele_{Phen}$. 1%), O_2 atmosphere ($Conv_{Trans}$. 97%, $Sele_{Cis}$. 44%, $Sele_{Byproduct}$. 20%, and $Sele_{Phen}$. 36%), and air atmosphere ($Conv_{Trans}$. 79%, $Sele_{Cis}$. 99%, and $Sele_{Phen}$. 1%) than that of **TPDT-COF**, which verifies the advantages of sevenfold interpenetrating 3D structure in photocatalysis. Besides, we have carefully searched

https://doi.org/10.1021/jacs.2c12313
J. Am. Chem. Soc. 2023, 145, 8860−8870

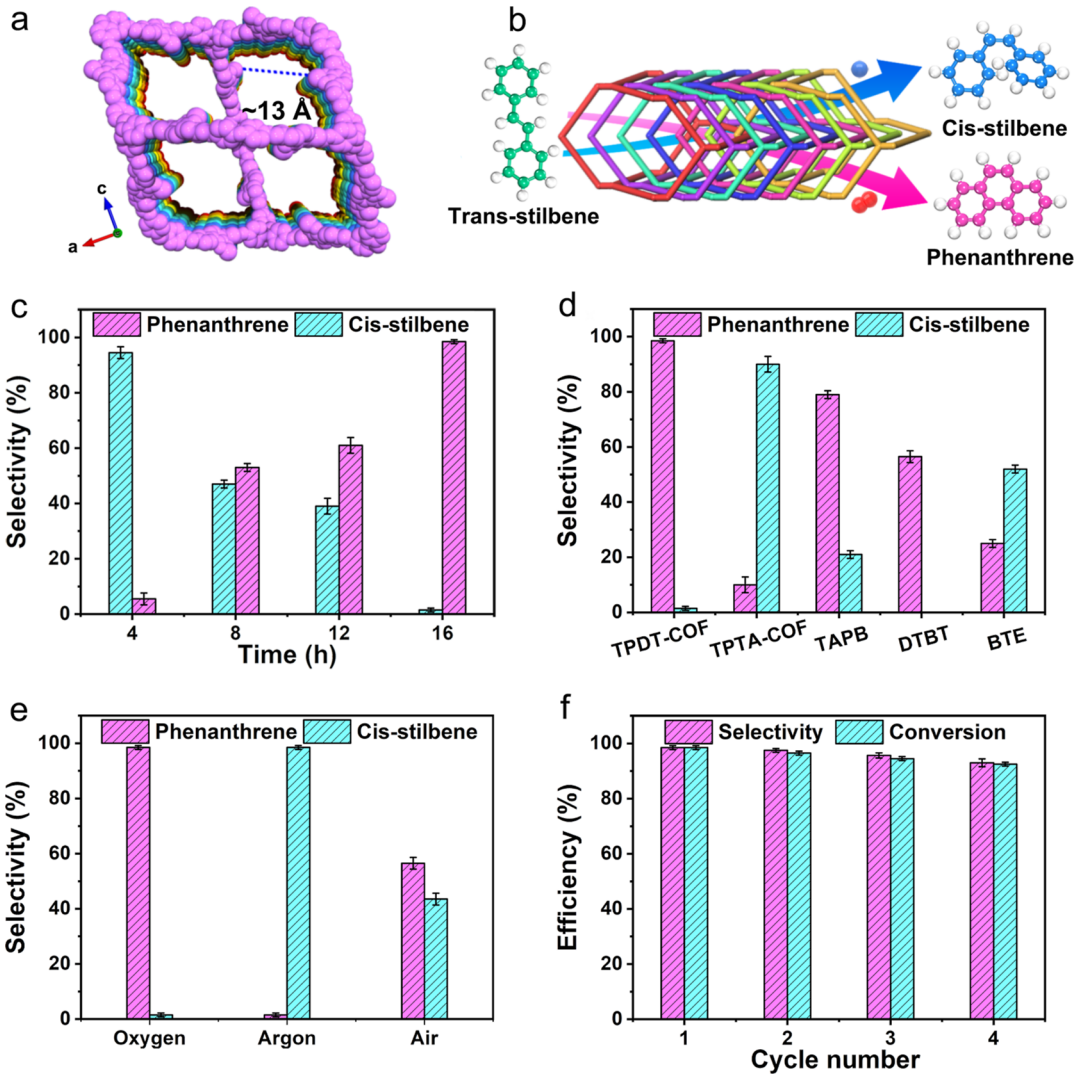

Figure 3. Photocatalytic performances of **TPDT-COF** and contrast samples in the photoisomerization and photocyclization of *trans*-stilbene. (a) Structural diagram in the different b axis of **TPDT-COF**. (b) Schematic diagram of the one-pot photoisomerization and photocyclization by **TPDT-COF**. (c) Time-dependent selectivity efficiency of *cis*-stilbene and phenanthrene for **TPDT-COF** under an O_2 atmosphere. (d) Photocatalytic performances of **TPDT-COF** and contrast samples. (e) Photocatalytic performances of **TPDT-COF** under different atmospheres. (f) Selectivity of products during the cycling tests for TPDT-COF under O_2 and Ar atmospheres.

related literature and selected some typical COFs to be compared with **TPDT-COF**. In detail, typical Wurster-motif COFs like **TAPD-(Me)$_2$-COF**, **TAPD-(OMe)$_2$-COF**, and **TAPP-TATA-COF** have been successfully synthesized referring to the reported literature and proved by PXRD tests, yet their performances were much inferior to that of **TPDT-COF** under different gas atmospheres (Figures S20 and S21).[51,65] In addition, 4,4′-(2,1,3-benzothiadiazole-4,7-diyl) bis-[benzaldehyde] (BTE), another chemical molecular that was similar to DTBT except that the benzothiadiazole group was absent, was also utilized as the contrast sample. As predicted, it displayed poorer properties ($Conv_{Trans}$. 88% and $Sele_{Phen}$. 24%) than those of DTBT and **TPDT-COF**, further proving the vital role of the benzothiadiazole group in the photocatalytic process. Based on the above-mentioned experimental results, it could be inferred that the covalent connection of TAPB and DTBT would generate efficient light-driven ligand-to-ligand charge transfer (LLCT effect) to facilitate the electron−hole separation/transfer to improve the photocatalysis for the improvement of photo-oxidation performance. Subsequently, the contrast test conditions (e.g., without light illumination and without both catalyst and light illumination) have been further evaluated, and they showed no reaction activity, demonstrating the vital role of light energy in photocatalytic reaction.

Based on the basic evaluation of performance for **TPDT-COF** under an O_2 atmosphere, we further set out to explore the potential effect of diverse gas atmospheres on photocatalytic properties. Under similar conditions, we further changed the gas atmosphere from O_2 to Ar and air (Figure 3e and Table S4). Under an Ar atmosphere, *cis*-stilbene could be hardly transformed into phenanthrene and most of the product was *cis*-stilbene ($Conv_{Trans}$. 88%, $Sele_{Cis}$. 99%, and $Sele_{Phen}$. 1%), which was completely different from that under an O_2 atmosphere ($Conv_{Trans}$. 100%, $Sele_{Phen}$. 99%, and $Sele_{Cis}$. 1%). Under an air atmosphere, it displayed the existence of both phenanthrene and *cis*-stilbene in the product ($Conv_{Trans}$. 91%, $Sele_{Phen}$. 56%, and $Sele_{Cis}$. 44%). Furthermore, we find that the low selectivity under the air atmosphere might be attributed to the low concentration of O_2 in the photocatalytic *trans*-stilbene

https://doi.org/10.1021/jacs.2c12313
J. Am. Chem. Soc. 2023, 145, 8860−8870

photoisomerization and photocyclization. In general, the content of N_2 in air is higher (78%) than that of O_2 (21%). To eliminate the influence of N_2, we conducted selective *trans*-stilbene photoisomerization and photocyclization under a N_2 atmosphere. The result showed a similar performance trend ($Conv_{Trans}$. 73%, $Sele_{Cis}$. 99%, and $Sele_{Phen}$. 1%) as that under an Ar atmosphere (Table S2). Moreover, **TPTA-COF** showed lower photoactivity than **TPDT-COF** under different atmospheres (i.e., O_2, Air, and Ar atmospheres) (Table S2), indicating that the DTBT unit and sevenfold interpenetrating structure played vital roles in photoisomerization or photocyclization. Based on the above results, we could conclude that the selective conversion of *trans*-stilbene to *cis*-stilbene or phenanthrene largely relied on the gas atmospheres and O_2 played a vital role in regulating the performance.

Cycling stability played a crucial role in assessing the durability of **TPDT-COF** during the photocatalytic process. To further investigate the cycling stability of **TPDT-COF**, we carried out recycling experiments under two different atmospheres (i.e., O_2 and Ar atmospheres). Remarkably, **TPDT-COF** could endure multiple cycling tests and both the conversion and selectivity remained almost unchanged at >4 cycles (Figure 3f). We also performed PXRD and FT-IR characterizations, and they proved the stability of the COF structure during the cycling tests (Figures S22 and S23). For the long-term recycling tests, we took the condition under an Ar atmosphere for instance and found that **TPDT-COF** could still exhibit >96% $Sele_{Cis.}$ with intact structure after more than 15 cycles (Figure S24).

To gain insight into the possible reaction process and reveal the reaction mechanism of the intermediate state, we performed controlled photocatalytic reactions using 4 equiv of a radical scavenger (2,2,6,6-tetramethyl-1-piperidinyloxy, TEMPO) to detect the specific effects of ROS (e.g., $^{\bullet}O_2^-$) produced in the photocatalytic process (Figure S25). When the gas atmosphere was O_2, the conversion and selectivity of phenanthrene significantly reduced under the optimal situations ($Conv_{Trans}$. 80%, $Sele_{Phen}$. 35%, and $Sele_{Cis}$. 65%) in the reaction medium, indicating that the photoreaction under the O_2 atmosphere was a ROS-mediated process. It was noted that no distinctive EPR signals were detected under ROS experimental conditions without illumination, demonstrating that $^{\bullet}O_2^-$ was generated under light illumination conditions. Moreover, the formation of superoxide $^{\bullet}O_2^-$ has also been confirmed, in which a characteristic EPR signal of $^{\bullet}O_2^-$ has also been detected in the EPR tests under the O_2 atmosphere (Figure S26). Similarly, $^{\bullet}O_2^-$ could also be detected with relative characteristic EPR signals under air atmospheres (Figure S27). However, the intensity was weaker than that under an O_2 atmosphere, indicating the vital role of O_2 concentration in adjusting the reaction efficiency. Interestingly, we found that a minor change in performance was detected with the same trapping agent (i.e., TEMPO) under the Ar atmosphere, suggesting that the reaction might not be mediated by $^{\bullet}O_2^-$ under argon. These results showed that the addition of O_2 was a crucial factor for product tuning from *cis*-stilbene to phenanthrene.

Based on the above results, we found that **TPDT-COF** had specific catalytic properties under different atmospheric conditions, which has been rarely reported to date. To investigate it, the effects of different gas atmospheres on product selectivity and catalytic mechanism were studied by DFT calculations under light illumination. The catalytic reaction mechanisms of **TPDT-COF** in highly selective *trans*-stilbene photoisomerization and photocyclization were studied by the free energy calculation (Figure 4a). The adsorption energy of *trans*-stilbene under O_2 (−0.65 eV) was much higher than those of vacuum (−0.44 eV) and the Ar atmosphere (−0.48 eV), indicating the stronger interaction of **TPDT-COF** with the substrate under the O_2 atmosphere. Besides, we found that DHP was the key intermediate in the process of selective *trans*-stilbene photoisomerization and photocyclization, in which the formation of DHP was the rate-determining step (RDS). First, we evaluated the effect of the catalyst on the RDS of DHP under vacuum and light conditions. We found that the energy barrier for DHP production under vacuum without a catalyst (1.44 eV) was much larger than the energy barrier in the presence of a catalyst (1.28 eV), showing the importance of **TPDT-COF** (Figure S28). In addition, we further set out to explore the effect of the gas atmosphere on photocatalytic performances by simulating three different gas atmospheres (i.e., vacuum, Ar, and O_2 atmospheres) in the possible photocatalytic pathways through DFT calculations (Figure 4a). It was noted that the energy barrier for the conversion of *cis*-stilbene to DHP followed the order of 1.38 eV (Ar) > 1.28 eV (vacuum) > 0.98 eV (O_2). Among them, the high-energy barrier for the conversion of *cis*-stilbene to DHP under the Ar atmosphere would set obstacles for further transformation from *cis*-stilbene to DHP, and thus, the *trans*-stilbene conversion was limited to *cis*-stilbene. For the condition under the O_2 atmosphere, the low energy barrier would make the *cis*-stilbene intermediate further transformed into the product phenanthrene. Therefore, the various gas atmospheres had a huge impact on the energy barrier of the RDS that could inherently determine the obvious performance change under different gas atmospheres during the photocatalytic processes. Besides, we also calculated the reaction mechanism of **TPTA-COF** under different gas atmospheres (Figure S29). The results showed that the reaction energy barriers of **TPTA-COF** were higher than that of **TPDT-COF** with lower adsorption capacity of the substrates, which complied with the poorer performance of **TPTA-COF** (Figure S29).

To reveal the vital role of the interpenetrating structure in photocatalysis, we further set out to study the possible pore confinement effect. In this work, the theoretical pore aperture of **TPDT-COF** was 12.31 Å × 17.99 Å. Based on our calculations, we found that the molecule size of *trans*-stilbene (7.04 Å × 14.76 Å) was slightly larger than the pore size if entered in one direction, while it could be accessible if it was vertical. In comparison, *cis*-stilbene (8.37 Å × 12.48 Å), the intermediate (DHP, 8.65 Å × 12.1 Å), and phenanthrene (8.39 Å × 12.38 Å) were all smaller in size than the pore aperture of **TPTA-COF**. Interestingly, due to the interpenetrating nature, the inner pore environment was irregular with the functional groups of DTBT protruding diagonally and pointed to the pore center, thus creating a complex and diversified environment with possible pore confinement effect for photocatalysis (Figure 1a). During the photocatalysis process, if the substrates interacted with the pore structures, the reaction might be largely restricted by the pore environment. To assess the importance of the interpenetrating structure in selective photoisomerization and photocyclization, we further studied the effect of molecular conformation on the photocatalytic reaction. 4,4′-Dimethyl-*trans*-stilbene, a derivative molecule with a larger molecule size (7.04 Å × 16.61 Å) than that of

https://doi.org/10.1021/jacs.2c12313
J. Am. Chem. Soc. 2023, 145, 8860−8870

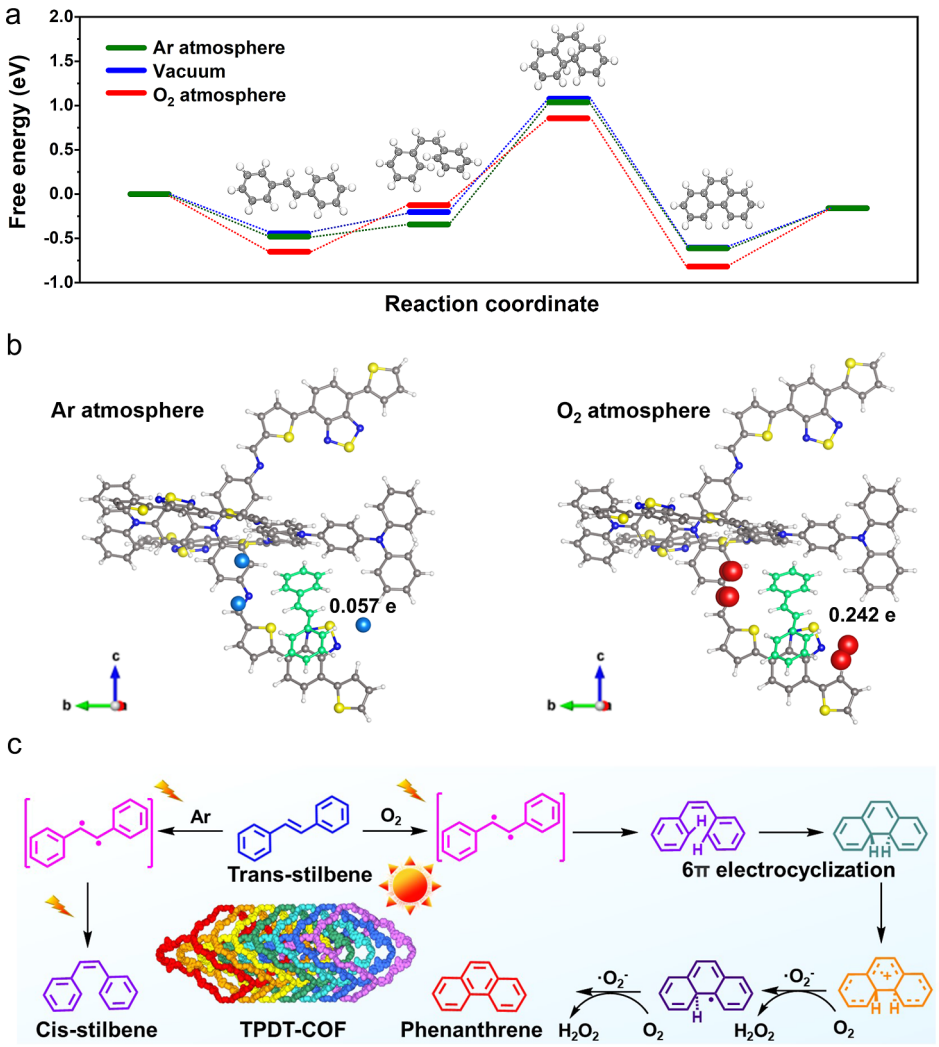

Figure 4. DFT calculations and the proposed reaction mechanism. (a) Free energy diagrams of the selective photoisomerization and photocyclization of **TPDT-COF** under different gas atmospheres (i.e., Ar, vacuum, and O_2). (b) Bader charge analysis of electron gained for *trans*-stilbene in **TPDT-COF** under Ar or O_2 atmospheres. (c) Schematic diagram of the possible mechanisms for selective photoisomerization and photocyclization.

trans-stilbene (7.04 Å × 14.76 Å), was selected and investigated under different gas atmospheres. Interestingly, it showed poorer performance under both Ar ($Conv_{Trans}$. 81% and $Sele_{Cis}$. 96%) and O_2 ($Conv_{Trans}$. 87% and $Sele_{Phen}$. 86%) atmospheres than *trans*-stilbene (Table S2). Based on the limited catalytic performance, we could conclude that the selective conversion of *trans*-stilbene to *cis*-stilbene or phenanthrene might be influenced by the steric hindrance caused by the pore confinement effect.

Furthermore, to confirm the catalytic effect of the sevenfold interpenetrating structure, we investigated it by combining Bader charge and differential charge density analyses to study the possible interactions between substrates and the pore structure. As shown in the Bader charge analysis of **TPDT-COF**, the positive value indicates gaining electrons, while the negative value means losing electrons. After calculations, the construction units (i.e., TAPB and DTBT) of **TPDT-COF** possessed varying interactions with the substrates or products. For the TAPB group, it was found that the N sites of TAPB had almost similar values for these compounds (i.e., *trans*-stilbene, 0.808 e; *cis*-stilbene, 0.803 e; DHP, 0.808 e, and phenanthrene, 0.808 e), implying that the TAPB unit might not be the active sites. As presented above, the TAPB unit with a Wurster-type structure could be transferred into a triple-excited state with double radical properties; thus, it would serve as the assisting group for photocatalysis. Notably, DTBT, another construction unit, possessed different interactions with these substrates, especially for the S sites (i.e., *trans*-stilbene, −0.715 e; *cis*-stilbene, −0.734 e; DHP, −0.699 e; and phenanthrene, −0.733 e) (Figure S30). Specifically, its interaction with *trans*-stilbene was much lower than those of *cis*-stilbene and phenanthrene, proving the more favorable and stable architectures of the products in the pore structure of **TPDT-COF**.

Then, we further performed the Bader charge analysis under different gas atmospheres to study the interaction at the molecular level using the interpenetrating structure fragment of **TPDT-COF** as the calculation model owing to the similar repeated unit in the interpenetrating COF structure (Figure 4b and S31). Under the O_2 atmosphere, the result shows that the −C═C− bond of *trans*-stilbene can get 0.242 e, which is higher than that under the Ar atmosphere (0.057 e). Meanwhile, under the O_2 atmosphere, the bond length of −C═C− was stretched longer (1.456 Å) than that under the

https://doi.org/10.1021/jacs.2c12313
J. Am. Chem. Soc. 2023, 145, 8860−8870

Ar atmosphere (1.358 Å). Therefore, the −C═C− bond of stilbene can easily enrich more electrons under the O_2 atmosphere than that under the Ar atmosphere, resulting in more easier isomerization and photocyclization for *trans*-stilbene. Based on the analysis results of differential charge density and Bader charge analysis, the gas atmospheres have a strong effect on interactions in the reaction, thus resulting in formation of different products. Similarly, to study the effect of gas change on the adsorbed substrates in **TPDT-COF**, we further conducted differential charge density analysis to analyze the possible interactions among the gas and −C═C− bond of stilbene and **TPDT-COF**. Initially, we calculated the differential charge density to analyze the possible interaction between the ligands in the interpenetrating **TPDT-COF** structure (Figure S32). It can be seen that electrons aggregate at the position of the interpenetrating junction of **TPDT-COF**, in which the red electron cloud indicates electron aggregation and the blue electron cloud indicates electron consumption. The difference in electron distribution will result in efficient charge transfer from the interpenetrating junction to other positions and possess an LLCT effect, which can accomplish selective *trans*-stilbene photoisomerization and photocyclization.

Based on the above experiments and analysis, a possible mechanism was proposed to illustrate the selective photoisomerization and photocyclization by **TPDT-COF** (Figure 4c) and is presented as follows. Driven by visible-light irradiation, the LLCT process takes place after absorbing photons. If it was under Ar conditions, **TPDT-COF** constructed by TAPB (light-absorption free radical generation) and the DTBT unit (catalytic unit) could induce the breakage of the π-bond to generate a biradical intermediate, which eventually rotated the C−C bond to generate *cis*-stilbene (Figure 4c). In contrast, if it was under O_2 conditions, the initial transformation from *trans*-stilbene to *cis*-stilbene might follow similar pathways.[32] Then, the generated $^{\bullet}O_2^-$ from O_2 would further induce the 6π electrocyclization of *cis*-stilbene to form the usually unstable and short-lived intermediate (DHP), which was finally oxidized with the assistance of $^{\bullet}O_2^-$ to generate phenanthrene.[11] During the processes, the sevenfold interpenetrating structure of **TPDT-COF** with pore confinement would also contribute to the successful transformation of *trans*-stilbene to *cis*-stilbene or phenanthrene, thus resulting in the unique and varying photocatalytic performances under different gas atmospheres.

CONCLUSIONS

In summary, a kind of sevenfold interpenetrating 3D COF (**TPDT-COF**) has been synthesized through the covalent coupling between TAPB and DTBT. Their synergistic integration endowed the interpenetrating porous structure with a pore confinement effect, visible-light-adsorption region, photoisomerization, and oxidative photocyclization ability. Noteworthily, it can achieve the photogeneration of *cis*-stilbene or phenanthrene with >99% selectivity by simply changing the gas atmosphere under mild photocatalysis conditions (Ar, $Sele_{Cis.}$ > 99%, $Sele_{Phen.}$ < 1% and O_2, $Sele_{Cis.}$ < 1%, and $Sele_{Phen.}$ > 99%). In this simple one-pot transformation process, the market value of *trans*-stilbene (~2,000 USD/kg) can be ~20 and ~35 times upgraded for *cis*-stilbene (~40,000 USD/kg) and phenanthrene (~70,000 USD/kg), respectively. Theoretical calculations prove the vital roles of the pore confinement effect and functional struts in **TPDT-COF** that joined together to achieve such unique photocatalytic performance. This work extends the considerable potential of COFs for selective stilbene photoisomerization and photocyclization, which might provide new insight into the design of efficient porous crystalline photocatalysts.

ASSOCIATED CONTENT

Supporting Information

The Supporting Information is available free of charge at https://pubs.acs.org/doi/10.1021/jacs.2c12313.

Detailed information regarding the experimental methods, characterization analysis, DFT calculations, and simulation for the theoretical COF structure (PDF)

AUTHOR INFORMATION

Corresponding Authors

Yifa Chen − *School of Chemistry, South China Normal University, Guangzhou 510006, PR China;* orcid.org/0000-0002-1718-6871; Email: chyf927821@163.com

Yong Yan − *School of Chemistry, South China Normal University, Guangzhou 510006, PR China;* orcid.org/0000-0002-7926-3959; Email: Yong.Yan@m.scnu.edu.cn

Ya-Qian Lan − *Jiangsu Collaborative Innovation Centre of Biomedical Functional Materials, Jiangsu Key Laboratory of New Power Batteries, School of Chemistry and Materials Science, Nanjing Normal University, Nanjing 210023, PR China; School of Chemistry, South China Normal University, Guangzhou 510006, PR China;* orcid.org/0000-0002-2140-7980; Email: yqlan@m.scnu.edu.cn, yqlan@njnu.edu.cn; http://www.yqlangroup.com

Authors

Tao-Yuan Yu − *Jiangsu Collaborative Innovation Centre of Biomedical Functional Materials, Jiangsu Key Laboratory of New Power Batteries, School of Chemistry and Materials Science, Nanjing Normal University, Nanjing 210023, PR China*

Qian Niu − *Jiangsu Collaborative Innovation Centre of Biomedical Functional Materials, Jiangsu Key Laboratory of New Power Batteries, School of Chemistry and Materials Science, Nanjing Normal University, Nanjing 210023, PR China*

Meng Lu − *School of Chemistry, South China Normal University, Guangzhou 510006, PR China*

Mi Zhang − *School of Chemistry, South China Normal University, Guangzhou 510006, PR China*

Jing-Wen Shi − *Jiangsu Collaborative Innovation Centre of Biomedical Functional Materials, Jiangsu Key Laboratory of New Power Batteries, School of Chemistry and Materials Science, Nanjing Normal University, Nanjing 210023, PR China*

Jiang Liu − *School of Chemistry, South China Normal University, Guangzhou 510006, PR China;* orcid.org/0000-0002-2596-4928

Shun-Li Li − *School of Chemistry, South China Normal University, Guangzhou 510006, PR China*

Complete contact information is available at: https://pubs.acs.org/10.1021/jacs.2c12313

Author Contributions

T.-Y.Y. and Q.N. contributed equally to this work. All authors discussed the results and commented on the manuscript.

Notes

The authors declare no competing financial interest.

■ ACKNOWLEDGMENTS

This work was financially supported by the NSFC (grants 22171139, 22225109, and 22071109), Natural Science Foundation of Guangdong Province (no. 2023B1515020076), Priority Academic Program Development of Jiangsu Higher Education Institutions, and the Foundation of Jiangsu Collaborative Innovation Center of Biomedical Functional Materials.

■ REFERENCES

(1) Molloy, J. J.; Schafer, M.; Wienhold, M.; Morack, T.; Daniliuc, C. G.; Gilmour, R. Boron-enabled geometric isomerization of alkenes via selective energy-transfer catalysis. *Science* **2020**, *369*, 302−306.
(2) Galego, J.; Garcia-Vidal, F. J.; Feist, J. Suppressing photochemical reactions with quantized light fields. *Nat. Commun.* **2016**, *7*, 13841.
(3) Raucci, U.; Weir, H.; Bannwarth, C.; Sanchez, D. M.; Martinez, T. J. Chiral photochemistry of achiral molecules. *Nat. Commun.* **2022**, *13*, 2091.
(4) Feng, G.; Gao, M.; Wang, L.; Chen, J.; Hou, M.; Wan, Q.; Lin, Y.; Xu, G.; Qi, X.; Chen, S. Dual-resolving of positional and geometric isomers of C=C bonds via bifunctional photocycloaddition-photoisomerization reaction system. *Nat. Commun.* **2022**, *13*, 2652.
(5) Song, D. H.; Yoo, H. Y.; Kim, J. P. Synthesis of stilbene-based azo dyes and application for dichroic materials in poly(vinyl alcohol) polarizing films. *Dyes. Pigm.* **2007**, *75*, 727−731.
(6) Hara, M.; Samori, S.; Cai, X.; Fujitsuka, M.; Majima, T. Importance of Properties of the Lowest and Higher Singlet Excited States on the Resonant Two-Photon Ionization of Stilbene and Substituted Stilbenes Using Two-Color Two-Lasers. *J. Phys. Chem. A* **2005**, *109*, 9831−9835.
(7) Hatarik, R.; Bernstein, L. A.; Caggiano, J. A.; Carman, M. L.; Schneider, D. H.; Zaitseva, N. P.; Wiedeking, M. Characterizing time decay of bibenzyl scintillator using time correlated single photon counting. *Rev. Sci. Instrum.* **2012**, *83*, 10D911.
(8) Molloy, J. J.; Morack, T.; Gilmour, R. Positional and Geometrical Isomerisation of Alkenes: The Pinnacle of Atom Economy. *Angew. Chem. Int. Ed.* **2019**, *58*, 13654−13664.
(9) Dugave, C.; Demange, L. Cis-Trans Isomerization of Organic Molecules and Biomolecules: Implications and Applications. *Chem. Rev.* **2003**, *34*, 2475−2532.
(10) Ioffe, I. N.; Granovsky, A. A. Photoisomerization of Stilbene: The Detailed XMCQDPT2 Treatment. *J. Chem. Theory. Comput.* **2013**, *9*, 4973−4990.
(11) Bao, J.; Minitti, M. P.; Weber, P. M. Ring-closing and dehydrogenation reactions of highly excited cis-stilbene: ultrafast spectroscopy and structural dynamics. *J. Phys. Chem. A.* **2011**, *115*, 1508−1515.
(12) Wittig, G.; Schöllkopf, U. Über Triphenyl-phosphin-methylene als olefinbildende Reagenzien (I. Mitteil.). *Chem. Ber.* **1954**, *87*, 1318−1330.
(13) Peterson, D. J. Carbonyl olefination reaction using silyl-substituted organometallic compounds. *J. Org. Chem.* **1968**, *33*, 780−784.
(14) Neumann, S. M.; Kochi, J. K. Synthesis of olefins. Cross-coupling of alkenyl halides and Grignard reagents catalyzed by iron complexes. *J. Org. Chem.* **1975**, *40*, 599−606.
(15) Meek, S. J.; O'Brien, R. V.; Llaveria, J.; Schrock, R. R.; Hoveyda, A. H. Catalytic Z-selective olefin cross-metathesis for natural product synthesis. *Nature* **2011**, *471*, 461−466.
(16) Maruoka, K.; Oishi, M.; Yamamoto, H. The Catalytic Shapiro Reaction. *J. Am. Chem. Soc.* **1996**, *118*, 2289−2290.
(17) Koh, M. J.; Khan, R. K.; Torker, S.; Hoveyda, A. H. Broadly applicable Z- and diastereoselective ring-opening/cross-metathesis catalyzed by a dithiolate ru complex. *Angew. Chem. Int. Ed.* **2014**, *53*, 1968−1972.
(18) Tsukamoto, T.; Dong, G. Catalytic Dehydrogenative Cyclization of o-Teraryls under pH-Neutral and Oxidant-Free Conditions. *Angew. Chem. Int. Ed.* **2020**, *59*, 15249−15253.
(19) Lamey, S. C.; Maloy, J. T. Ultrapurification of Aromatic Hydrocarbons through Liquid-Liquid Extraction with Sulfuric Acid. *J. Sep. Sci.* **2006**, *9*, 391−400.
(20) Liou, Y.; Chang, C. J. Separation of Anthracene from Crude Anthracene Using Gas Antisolvent Recrystallization. *Sep. Sci. Technol.* **1992**, *27*, 1277−1289.
(21) Jorgensen, K. B. Photochemical oxidative cyclisation of stilbenes and stilbenoids-the Mallory-reaction. *Molecules* **2010**, *15*, 4334−4358.
(22) Lvov, A. G. Switching the Mallory Reaction to Synthesis of Naphthalenes, Benzannulated Heterocycles, and Their Derivatives. *J. Org. Chem.* **2020**, *85*, 8749−8759.
(23) Chakraborty, S.; Saha, C. A Tribute to Bardhan and Sengupta. *Resonance* **2015**, *20*, 628−642.
(24) Zhai, L.; Shukla, R.; Wadumethrige, S. H.; Rathore, R. Probing the arenium-ion (protontransfer) versus the cation-radical (electron transfer) mechanism of Scholl reaction using DDQ as oxidant. *J. Org. Chem.* **2010**, *75*, 4748−4760.
(25) King, B. T.; Kroulík, J.; Robertson, C. R.; Rempala, P.; Hilton, C. L.; Korinek, J. D.; Gortari, L. M. Controlling the Scholl Reaction. *J. Org. Chem.* **2007**, *72*, 2279−2288.
(26) Dou, X.; Yang, X.; Bodwell, G. J.; Wagner, M.; Enkelmann, V.; Müllen, K. Unexpected Phenyl Group Rearrangement during an Intramolecular Scholl Reaction Leading to an Alkoxy-Substituted Hexa-peri-hexabenzocoronene. *Org Lett* **2007**, *9*, 2485−2488.
(27) Li, H.; He, K. H.; Liu, J.; Wang, B. Q.; Zhao, K. Q.; Hu, P.; Shi, Z. J. Straightforward synthesis of phenanthrenes from styrenes and arenes. *Chem. Commun.* **2012**, *48*, 7028−7030.
(28) Matsushima, T.; Kobayashi, S.; Watanabe, S. Air-Driven Potassium Iodide-Mediated Oxidative Photocyclization of Stilbene Derivatives. *J. Org. Chem.* **2016**, *81*, 7799−7806.
(29) Nevesely, T.; Wienhold, M.; Molloy, J. J.; Gilmour, R. Advances in the E -> Z Isomerization of Alkenes Using Small Molecule Photocatalysts. *Chem. Rev.* **2022**, *122*, 2650−2694.
(30) Matsuura, R.; Karunananda, M. K.; Liu, M.; Nguyen, N.; Blackmond, D. G.; Engle, K. M. Mechanistic Studies of Pd(II)-Catalyzed E/Z Isomerization of Unactivated Alkenes: Evidence for a Monometallic Nucleopalladation Pathway. *ACS Catal* **2021**, *11*, 4239−4246.
(31) Metternich, J. B.; Gilmour, R. A Bio-Inspired, Catalytic E -> Z Isomerization of Activated Olefins. *J. Am. Chem. Soc.* **2015**, *137*, 11254−11257.
(32) Fabry, D. C.; Ronge, M. A.; Rueping, M. Immobilization and continuous recycling of photoredox catalysts in ionic liquids for applications in batch reactions and flow systems: catalytic alkene isomerization by using visible light. *Chem.—Eur. J.* **2015**, *21*, 5350−5354.
(33) Metternich, J. B.; Artiukhin, D. G.; Holland, M. C.; von Bremen-Kuhne, M.; Neugebauer, J.; Gilmour, R. Photocatalytic E -> Z Isomerization of Polarized Alkenes Inspired by the Visual Cycle: Mechanistic Dichotomy and Origin of Selectivity. *J. Org. Chem.* **2017**, *82*, 9955−9977.
(34) Xu, J.; Liu, N.; Lv, H.; He, C.; Liu, Z.; Shen, X.; Cheng, F.; Fan, B. Photocatalyst-free visible light promoted E -> Z isomerization of alkenes. *Green Chem* **2020**, *22*, 2739−2743.
(35) Cai, W.; Fan, H.; Ding, D.; Zhang, Y.; Wang, W. Synthesis of Z-alkenes via visible light promoted photocatalytic E -> Z isomerization under metal-free conditions. *Chem. Commun.* **2017**, *53*, 12918−12921.
(36) Nakatani, K.; Sato, H.; Fukuda, R. A catalyzed E/Z isomerization mechanism of stilbene using para-benzoquinone as a triplet sensitizer. *Phys. Chem.* **2022**, *24*, 1712−1721.
(37) Metternich, J. B.; Sagebiel, S.; Lückener, A.; Lamping, S.; Ravoo, B. J.; Gilmour, R. Covalent Immobilization of (-)-Riboflavin

https://doi.org/10.1021/jacs.2c12313
J. Am. Chem. Soc. 2023, 145, 8860−8870

on Polymer Functionalized Silica Particles: Application in the Photocatalytic E -> Z Isomerization of Polarized Alkenes. *Chem.—Eur. J.* **2018**, *24*, 4228−4233.
(38) Frederick, J. H.; Fujiwara, Y.; Penn, J. H.; Yoshihara, K.; Petek, H. Models for stilbene photoisomerization: experimental and theoretical studies of the excited-state dynamics of 1,2-diphenylcycloalkenes. *J. Phys. Chem.* **1991**, *95*, 2845−2858.
(39) Staden, L. F. v.; Gravestock, D.; Ager, D. J. New developments in the Peterson olefination reaction. *Chem. Soc. Rev.* **2002**, *31*, 195−200.
(40) Negishi, E.; Huang, Z.; Wang, G.; Mohan, S.; Wang, C.; Hattori, H. Recent Advances in Efficient and Selective Synthesis of Di-Tri-and Tetrasubstituted Alkenes via Pd-Catalyzed Alkenylation-Carbonyl Olefination Synergy. Accounts. *Chem. Res.* **2008**, *41*, 1474−1485.
(41) Endo, K.; Grubbs, R. H. Chelated ruthenium catalysts for Z-selective olefin metathesis. *J. Am. Chem. Soc.* **2011**, *133*, 8525−8527.
(42) Lewis, F. D.; Yoon, B. A.; Arai, T.; Iwasaki, T.; Tokumaru, K. Molecular Structure and Photochemistry of (E)- and (Z)-2-(2-(2-Pyridyl) ethenyl) indole. A Case of Hydrogen Bond Dependent One-Way Photoisomerization. *J. Am. Chem. Soc.* **1995**, *117*, 3029−3036.
(43) Waldeck, D. H. Photoisomerization Dynamics of Stilbenes. *Chem. Rev.* **1991**, *91*, 415−436.
(44) Liu, M.; Chen, Y. J.; Huang, X.; Dong, L. Z.; Lu, M.; Guo, C.; Yuan, D.; Chen, Y.; Xu, G.; Li, S. L.; Lan, Y. Q. Porphyrin-Based COF 2D Materials: Variable Modification of Sensing Performances by Post-Metallization. *Angew. Chem. Int. Ed.* **2022**, *134*, No. e202115308.
(45) Lu, M.; Liu, J.; Li, Q.; Zhang, M.; Liu, M.; Wang, J. L.; Yuan, D. Q.; Lan, Y. Q. Rational Design of Crystalline Covalent Organic Frameworks for Efficient CO_2 Photoreduction with H_2O. *Angew. Chem. Int. Ed.* **2019**, *131*, 12522−12527.
(46) Liu, R.; Tan, K. T.; Gong, Y.; Chen, Y.; Li, Z.; Xie, S.; He, T.; Lu, Z.; Yang, H.; Jiang, D. Covalent organic frameworks: an ideal platform for designing ordered materials and advanced applications. *Chem. Soc. Rev.* **2021**, *50*, 120−242.
(47) Wang, K.; Kang, X.; Yuan, C.; Han, X.; Liu, Y.; Cui, Y. Porous 2D and 3D Covalent Organic Frameworks with Dimensionality-Dependent Photocatalytic Activity in Promoting Radical Ring-Opening Polymerization. *Angew. Chem. Int. Ed.* **2021**, *60*, 19466−19476.
(48) Li, S.; Li, L.; Li, Y.; Dai, L.; Liu, C.; Liu, Y.; Li, J.; Lv, J.; Li, P.; Wang, B. Fully Conjugated Donor-Acceptor Covalent Organic Frameworks for Photocatalytic Oxidative Amine Coupling and Thioamide Cyclization. *ACS Catal* **2020**, *10*, 8717−8726.
(49) Yang, Y.; Yu, L.; Chu, T.; Niu, H.; Wang, J.; Cai, Y. Constructing chemical stable 4-carboxyl-quinoline linked covalent organic frameworks via Doebner reaction for nanofiltration. *Nat. Commun.* **2022**, *13*, 2615.
(50) Bhadra, M.; Kandambeth, S.; Sahoo, M. K.; Addicoat, M.; Balaraman, E.; Banerjee, R. Triazine Functionalized Porous Covalent Organic Framework for Photo-organocatalytic E- Z Isomerization of Olefins. *J. Am. Chem. Soc.* **2019**, *141*, 6152−6156.
(51) Krishnaraj, C.; Sekhar Jena, H.; Bourda, L.; Laemont, A.; Pachfule, P.; Roeser, J.; Chandran, C. V.; Borgmans, S.; Rogge, S. M. J.; Leus, K.; Stevens, C. V.; Martens, J. A.; Van Speybroeck, V.; Breynaert, E.; Thomas, A.; Van Der Voort, P. Strongly Reducing (Diarylamino)benzene-Based Covalent Organic Framework for Metal-Free Visible Light Photocatalytic H_2O_2 Generation. *J. Am. Chem. Soc.* **2020**, *142*, 20107−20116.
(52) Störle, C.; Eyer, P. Reactions of The Wurster's Blue Radical Cation with Thiols, and Some Properties of The Reaction Products. *Chem. Biol. Interact.* **1991**, *78*, 333−346.
(53) Uebe, M.; Kato, T.; Tanaka, K.; Ito, A. 9,10-Diaminoanthracenes Revisited: The Influence of N-Substituents on Their Electronic States. *Chem.—Eur. J.* **2016**, *22*, 18923−18931.
(54) Elewa, A. M.; Elsayed, M. H.; EL-Mahdy, A. F.; Chang, C. L.; Ting, L. Y.; Lin, W. C.; Lu, C. Y.; Chou, H. H. Triptycene-based discontinuously-conjugated covalent organic polymer photocatalysts for visible-light-driven hydrogen evolution from water. *Appl. Catal. B* **2021**, *285*, 119802.
(55) Sun, D.; Ke, Y.; Mattox, T. M.; Ooro, B. A.; Zhou, H. C. Temperature-dependent supramolecular stereoisomerism in porous copper coordination networks based on a designed carboxylate ligand. *Chem. Commun.* **2005**, *43*, 5447−5449.
(56) Li, X.; Liu, J.; Zhou, K.; Ullah, S.; Wang, H.; Zou, J.; Thonhauser, T.; Li, J. Tuning Metal-Organic Framework (MOF) Topology by Regulating Ligand and Secondary Building Unit (SBU) Geometry: Structures Built on 8-Connected M(6) (M = Zr, Y) Clusters and a Flexible Tetracarboxylate for Propane-Selective Propane/Propylene Separation. *J. Am. Chem. Soc.* **2022**, *144*, 21702−21709.
(57) Xia, C.; Kirlikovali, K. O.; Nguyen, T. H. C.; Nguyen, X. C.; Tran, Q. B.; Duong, M. K.; Nguyen Dinh, M. T.; Nguyen, D. L. T.; Singh, P.; Raizada, P.; Nguyen, V.-H.; Kim, S. Y.; Singh, L.; Nguyen, C. C.; Shokouhimehr, M.; Le, Q. V. The emerging covalent organic frameworks (COFs) for solar-driven fuels production. *Coord. Chem. Rev.* **2021**, *446*, 214117.
(58) Yang, R.-X.; Wang, Y.-R.; Gao, G.-K.; Chen, L.; Chen, Y.; Li, S.-L.; Lan, Y.-Q. Self-Assembly of Hydroxyl Metal-Organic Polyhedra and Polymer into Cu-Based Hollow Spheres for Product-Selective CO_2. *Electroreduction. Small Struct.* **2021**, *2*, 2100012.
(59) Hao, Q.; Li, Z. J.; Bai, B.; Zhang, X.; Zhong, Y. W.; Wan, L. J.; Wang, D. A Covalent Organic Framework Film for Three-State Near-Infrared Electrochromism and a Molecular Logic Gate. *Angew. Chem. Int. Ed.* **2021**, *133*, 12606−12611.
(60) Nouruzi, N.; Dinari, M.; Gholipour, B.; Mokhtari, N.; Farajzadeh, M.; Rostamnia, S.; Shokouhimehr, M. Photocatalytic hydrogen generation using colloidal covalent organic polymers decorated bimetallic Au-Pd nanoalloy (COPs/Pd-Au). *Mol. Catal.* **2022**, *518*, 112058.
(61) Jiang, C.; Zhang, Y.; Zhang, M.; Ma, N.-N.; Gao, G.-K.; Wang, J.-H.; Zhang, M.-M.; Chen, Y.; Li, S.-L.; Lan, Y.-Q. Exfoliation of covalent organic frameworks into MnO_2-loaded ultrathin nanosheets as efficient cathode catalysts for Li-CO_2 batteries. *Cell Rep. Phys. Sci.* **2021**, *2*, 100392.
(62) Zhang, K.; Kirlikovali, K. O.; Varma, R. S.; Jin, Z.; Jang, H. W.; Farha, O. K.; Shokouhimehr, M. Covalent Organic Frameworks: Emerging Organic Solid Materials for Energy and Electrochemical Applications. *ACS Appl. Mater. Interfaces* **2020**, *12*, 27821−27852.
(63) Lee, M. K.; Shokouhimehr, M.; Kim, S. Y.; Jang, H. W. Two-Dimensional Metal−Organic Frameworks and Covalent−Organic Frameworks for Electrocatalysis: Distinct Merits by the Reduced Dimension. *Adv. Energy Mater.* **2021**, *12*, 2003990.
(64) Chang, J. N.; Li, Q.; Yan, Y.; Shi, J.; Zhou, J.; Lu, M.; Zhang, M.; Ding, H.; Chen, Y.; Li, S.; et al. Covalent-Bonding Oxidation Group and Titanium Cluster to Synthesize a Porous Crystalline Catalyst for Selective Photo-Oxidation Biomass Valorization. *Angew. Chem. Int. Ed.* **2022**, *61*, No. e202209289.
(65) Liu, M.; Liu, S.; Cui, C. X.; Miao, Q.; He, Y.; Li, X.; Xu, Q.; Zeng, G. Construction of Catalytic Covalent Organic Frameworks with Redox-Active Sites for the Oxygen Reduction and the Oxygen Evolution Reaction. *Angew. Chem. Int. Ed.* **2022**, *134*, No. e202213522.

https://doi.org/10.1021/jacs.2c12313
J. Am. Chem. Soc. 2023, 145, 8860−8870